Biomaterials Science

ROYAL SOCIETY OF CHEMISTRY

PAPER

View Article Online
View Journal | View Issue

Check for updates

Cite this: *Biomater. Sci.*, 2024, **12**, 2149

Design, manufacturing and testing of a green non-isocyanate polyurethane prosthetic heart valve†

Sofia F. Melo,[a] Alicia Nondonfaz,[a] Abdelhafid Aqil,[b] Anna Pierrard,[b] Alexia Hulin,[a] Céline Delierneux,[a] Bartosz Ditkowski,[a] Maxime Gustin,[a] Maxime Legrand,[c] Bibian M. E. Tullemans,[d] Sanne L. N. Brouns,[d] Alain Nchimi,[a] Raoul Carrus,[c] Astrid Dejosé,[c] Johan W. M. Heemskerk,[d] Marijke J. E. Kuijpers,[d] Jan Ritter,[e] Ulrich Steinseifer,[e] Johanna C. Clauser,[e] Christine Jérôme,[b] Patrizio Lancellotti‡[a] and Cécile Oury *‡[a]

Received 23rd November 2023,
Accepted 6th March 2024

DOI: 10.1039/d3bm01911j

rsc.li/biomaterials-science

The sole effective treatment for most patients with heart valve disease is valve replacement by implantation of mechanical or biological prostheses. However, mechanical valves represent high risk of thromboembolism, and biological prostheses are prone to early degeneration. In this work, we aim to determine the potential of novel environmentally-friendly non-isocyanate polyurethanes (NIPUs) for manufacturing synthetic prosthetic heart valves. Polyhydroxyurethane (PHU) NIPUs are synthesized *via* an isocyanate-free route, tested *in vitro*, and used to produce aortic valves. PHU elastomers reinforced with a polyester mesh show mechanical properties similar to native valve leaflets. These NIPUs do not cause hemolysis. Interestingly, both platelet adhesion and contact activation-induced coagulation are strongly reduced on NIPU surfaces, indicating low thrombogenicity. Fibroblasts and endothelial cells maintain normal growth and shape after indirect contact with NIPUs. Fluid-structure interaction (FSI) allows modeling of the ideal valve design, with minimal shear stress on the leaflets. Injection-molded valves are tested in a pulse duplicator and show ISO-compliant hydrodynamic performance, comparable to clinically-used bioprostheses. Poly(tetrahydrofuran) (PTHF)-NIPU patches do not show any evidence of calcification over a period of 8 weeks. NIPUs are promising sustainable biomaterials for the manufacturing of improved prosthetic valves with low thrombogenicity.

1. Introduction

One of the most common valvular heart disease is aortic stenosis, which affects 3–6% of the population over 65 years old,[1] overall impacting more than 40 million people worldwide. Valve replacement with prosthetic heart valves has shown to substantially improve survival in patients, and is currently considered the effective treatment for aortic valve disease,[2,3] with approximately 300 000 prosthetic heart valves being implanted every year (850 000 are expected by 2050).[4,5] Clinically available prosthetic heart valves include mechanical and biological valves (bioprostheses). Despite recent structural and hemodynamic improvements, the available options are still far from an optimal solution. This is mainly due to the need for constant administration of anticoagulant drugs when mechanical valves are implanted, and to progressive structural deterioration in the case of bioprostheses, which then requires reoperation.[6]

Synthetic heart valves made from polymer-based materials have long been considered as potential alternatives to the traditional prostheses.[7,8] Polyurethanes (PUs), typically produced by reacting isocyanates with polyols, have been a popular choice for heart valve-related research,[9] given their appropriate mechanical properties.[10–12] PUs are used in several medical applications such as intravascular catheters and extracorporeal circuits. However, regarding heart valves, the evaluation of various PUs revealed problems associated with long-term implantation, including thrombotic events,[13,14] calcification[15–20] and sub-optimal valve geometry issues.[21–23] Recent research on prosthetic valves focused on applying modifications to PU,[10,24] and different research groups

[a]*Laboratory of Cardiology, GIGA-Cardiovascular Sciences, University of Liège, Avenue de l'Hôpital 11, B34, 4000 Liège, Belgium. E-mail: cecile.oury@uliege.be*
[b]*Center for Education and Research on Macromolecules (CERM), CESAM Research Unit, Department of Chemistry, University of Liège, Allée du 6 août 13, B6a, 4000 Liège, Belgium*
[c]*Sirris, Liège Science Park, Rue du Bois Saint-Jean 12, 4102 Seraing, Belgium*
[d]*Cardiovascular Research Institute Maastricht (CARIM), Department of Biochemistry, Maastricht University, Universiteitssingel 50, 6200 MD Maastricht, The Netherlands*
[e]*Department of Cardiovascular Engineering, Institute of Applied Medical Engineering, Medical Faculty RWTH Aachen University, Pauwelsstraße 20, 52074 Aachen, Germany*

†Electronic supplementary information (ESI) available. See DOI: https://doi.org/10.1039/d3bm01911j

‡Authors contributed equally to this work.

reported *in vitro* and *in vivo* tests with valves made of polycarbonate urethane (PCU),[20,25] composites thereof,[26–29] and siloxane-based PUs.[30,31] In 2021, Foldax used the LifePolymer™, a siloxane poly(urethane–urea) (SiPUU), to develop the Tria valve, the first polymeric valve implanted in patients.[24] However, long-term prosthesis performance has not been demonstrated yet.

Additionally, conventional PU production involves toxic isocyanates harmful to human health (often triggering severe asthma and dermatitis). The European Chemicals Agency has therefore emitted restrictions for its use.[32–34] The aim of the present study was to develop and test novel environmentally-friendly non-isocyanate PUs (NIPUs) as potential biomaterials for heart valves. A key advantage of NIPUs lays on the use of CO_2 during the first synthesis step, which contributes to recycling this waste product.

In this work (Scheme 1), we synthesized new NIPUs *via* ring-opening conjugation of bis(cyclic carbonate)s (bisCC) and polyamines, in an isocyanate-free route. We demonstrated NIPUs hemo/biocompatibility and low thrombogenicity, as shown by extremely low platelet adhesion on NIPU surfaces. We then developed a 3D fluid-structure interaction (FSI) model to design NIPU valves. After achieving ideal valve design, we successfully produced injection-molded valves and verified their ISO-compliant hydrodynamic performances in a pulse duplicator, which validated the *in silico* simulation. Calcification on NIPU patches was evaluated over 8 weeks, showing no calcifying profile. Our study is the first report on the use of NIPUs for manufacturing prosthetic heart valves.

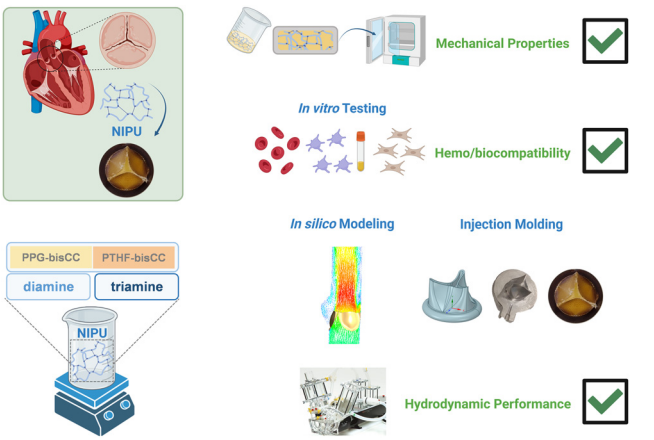

Scheme 1 Development of NIPU aortic heart valves: polymer synthesis, mechanical and biological testing, valve design, fabrication, and evaluation in a pulse duplicator.

2. Results

2.1 Synthesis and characterization of NIPU precursors and networks

Conversion of poly(propylene glycol) diglycidyl ether (PPG DE) and poly(tetrahydrofuran) di-epoxide (PTHF DE) into poly(propylene glycol) bis(cyclic carbonate) (PPG bisCC) and poly(tetrahydrofuran) bis(cyclic carbonate) (PTHF bisCC) was confirmed in the NMR spectra, as shown by disappearance of the bands corresponding to epoxy groups in the range of 2.6–3.2 ppm and appearance of bands assigned to cyclic carbonates at 4.5 and 4.8 ppm (Fig. S1A and S1B†). PPG bisCC and PTHF bisCC were reacted with 4-((4-aminocyclohexyl)methyl)-cyclohexanamine (MBCHA) and *N*′,*N*′-bis(2-aminoethyl)ethane-1,2-diamine (TAEA) to form cross-linked PPG-NIPU and PTHF-NIPU networks. These NIPUs were solid and flexible materials (elastomers), as shown in Fig. S2.† Thermal properties, contact angles, water uptake and swelling behaviors, as well as mechanical properties of the materials were assessed (Table 1). Glass-transition temperatures (T_gs) were measured for PPG-NIPU and PTHF-NIPU, yielding negative temperatures: −1.2 °C and −48.9 °C, respectively. Above these temperatures ($T > T_g$), the polymers had a viscoelastic (rubbery) behavior. Contact angle measurements on PPG-NIPU and PTHF-NIPU surfaces revealed values of 55.3° and 42.5°, respectively, indicative of hydrophilic polymers, which translated into high equilibrium water absorption (EWA): 26.21% for PPG-NIPU and 14.91% for PTHF-NIPU. Maximum expansion percentages of 9.49% and 9.05% were found for PPG-NIPU and PTHF-NIPU. Considering the differences observed before and after hydration, the mechanical properties of our NIPUs, namely elastic modulus (E), ultimate tensile strength (σ_r) and fracture

Table 1 Measurements of glass-transition temperature, contact angle, EWA, expansion and mechanical properties (mean ± SD, n = 3) of the synthesized polymers

Material	T_g (°C)	Contact angle (°)	EWA (%)	Expansion[a] (%)	E (MPa)	σ_r (MPa)	ε_r (%)
PPG-NIPU	−1.2	55.3	26.21	9.49/8.53/8.15	Dry: 15.62 ± 3.93 Wet: 1.51 ± 0.25	Dry: 1.44 ± 0.09 Wet: 0.17 ± 0.11	Dry: 233.9 ± 15.04 Wet: 16.7 ± 5.7
PTHF-NIPU	−48.9	42.5	14.91	2.72/6.26/9.05	Dry: 1.81 ± 0.16 Wet: 1.22 ± 0.06	Dry: 0.78 ± 0.07 Wet: 0.44 ± 0.09	Dry: 104.8 ± 13.5 Wet: 61.8 ± 12.4
PPG-NIPU + PET reinforcement	—	—	36.76	23.54/9.96/8.75	Dry: 73.00 ± 19.51 Wet: 3.39 ± 1.01	Dry: 1.79 ± 0.10 Wet: 0.79 ± 0.37	Dry: 20.4 ± 11.9 Wet: 83.9 ± 31.9
PTHF-NIPU + PET reinforcement	—	—	9.01	6.78/4.58/1.05	Dry: 4.62 ± 0.98 Wet: 4.67 ± 0.60	Dry: —[b] Wet: —[b]	Dry: —[b] Wet: —[b]

[a] Dimensions: thickness/width/length. [b] Test stopped before break: maximum tensile capacity of load cells was reached.

strain (ε_r), were measured in both dry and wet states. PPG-NIPU showed more important alterations than PTHF-NIPU, with E dropping from 15.62 ± 3.93 MPa (dry) to 1.51 ± 0.25 MPa (wet), σ_r from 1.44 ± 0.09 to 0.17 ± 0.11 MPa, and ε_r decreasing from 233.9 ± 15.04% to 16.7 ± 5.7%. PTHF-NIPU showed less differences between dry and wet state than PPG-NIPU. A poly(ethylene terephthalate) (PET) mesh (Dacron 3002, Surgical Mesh™) was incorporated in our NIPU networks to reinforce them. The addition of PET resulted in increased E values for wet samples (3.39 ± 1.01 MPa for PPG-NIPU + PET and 4.67 ± 0.60 MPa for PTHF-NIPU + PET). For PPG-NIPU + PET, σ_r and ε_r also increased to 0.79 ± 0.37 MPa and 83.9 ± 31.9% in wet conditions. For PTHF-NIPU + PET, σ_r and ε_r could not be determined since the test ended before a clear break was observed, confirming the mechanical advantage brought by PET incorporation. Unexpectedly, the incorporation of PET caused an increase in both EWA and expansion percentages for PPG-NIPU networks, while this negative impact was not observed for PTHF-NIPU. We thus succeeded to synthesize two NIPU elastomers with mechanical properties similar to the ones of native valve leaflets[35,36] upon reinforcement with a PET mesh.

The absence of degradation of NIPUs was evaluated after 14 days of immersion in a phosphate buffered saline (PBS) solution. We did not observe any modification of the pH of the solution that varied from 7.23 to 7.29 for PPG-NIPU and from 7.27 to 7.32 for PTHF-NIPU. The morphology of the NIPU specimens remained intact with no discoloration or cracking phenomena. Thermal analysis by differential scanning calorimetry (DSC) was also carried out on day 14, showing no changes in the NIPUs properties. T_g values of −1.1 °C and −52.3 °C were found for PPG-NIPU and PTHF-NIPU, respectively, compared to −1.2 °C and −48.9 on day 0.

2.2 Low *in vitro* thrombogenicity of NIPU elastomers

We evaluated the hemocompatibility of the two NIPUs in hemolysis tests (Fig. 1A). According to ASTM F756-00 criteria, both PPG-NIPU and PTHF-NIPU were non-hemolytic (with mean hemolysis rates of −0.2 ± 0.15% and 0.5 ± 0.31%, respectively). The mean hemolysis rate of our PU reference was 0.2 ± 0.22%, which was slightly higher than PPG-NIPU (p = 0.04) and similar to that of PTHF-NIPU.

Platelet adhesion on NIPU surface (Fig. 1B) was then evaluated using lactate dehydrogenase (LDH) activity assays. Mean values of absorbance ($\lambda \approx 450$ nm) for PU, PPG-NIPU and PTHF-NIPU were 1.55 ± 0.41, 0.24 ± 0.03 and 0.20 ± 0.06, respectively. These data showed that medical grade PU promoted significantly more platelet adhesion on its surface than our two NIPUs ($p < 0.001$). To further explore this interesting observation under conditions that mimic the heart valve environment, human whole blood was perfused under flow over coverslips coated with PU and NIPUs, following an experimental set-up that evaluates thrombus formation at arterial shear rates.[37] Our results (Fig. S7†) showed a mean platelet surface coverage of 1.30 ± 1.44% for PU, and lower values of 0.11 ± 0.19% for PPG-NIPU (p = 0.04) and 0.58 ± 0.59% for PTHF-NIPU. Our data therefore indicated lower platelet adhesion on NIPU surfaces than on medical grade PU under flow.

Contact activation of the coagulation cascade was studied using the non-activated partial thromboplastin time (NaPTT) test (Fig. 1C). Plasma incubated with PPG-NIPU and PTHF-NIPU showed similar mean clotting times (240 ± 17 s and 224 ± 17 s, respectively) that did not differ from that obtained with plasma alone (mean of 250 ± 18 s). Interestingly, conventional PU reference triggered significantly shorter clot-

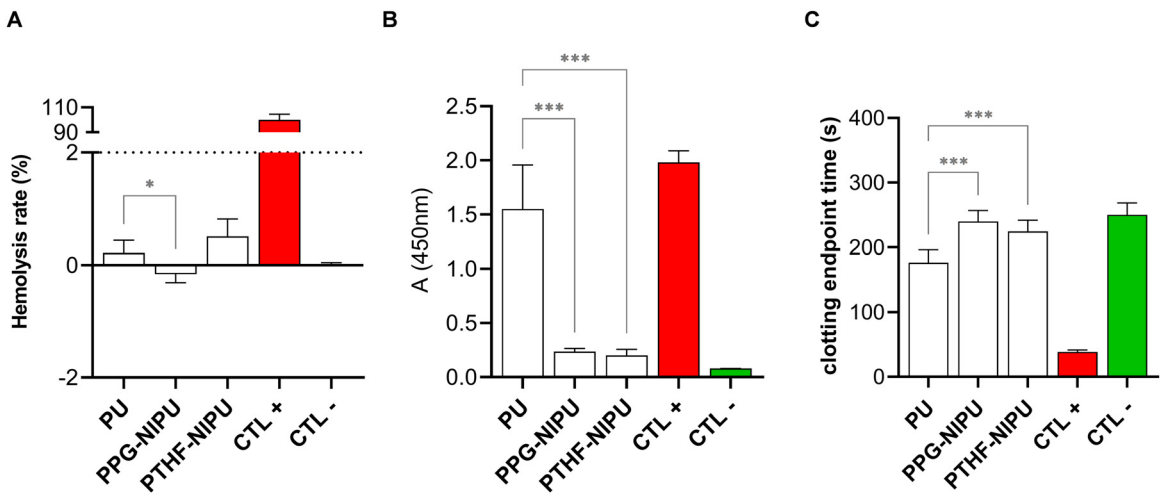

Fig. 1 *In vitro* hemocompatibility assessment. (A) Hemolysis rate in red blood cells (RBCs) after 3 h of incubation with PU/NIPU discs. A solution of 1 : 7 RBCs/distilled water was used as CTL+, while a solution of 1 : 7 RBCs/PBS was the CTL−; (B) LDH activity of adhered human platelets after 2 h of incubation with PU/NIPU discs, assessed by a colorimetric assay. CTL+ and CTL− are provided with the Sigma-Aldrich assay kit; (C) clotting times of platelet-poor plasma after 2 h of incubation with PU/NIPU discs. Kaolin-coated glass coverslips were used as CTL+, while platelet-poor plasma (PPP) alone was used as CTL−. Data are presented as mean with SD (n = 3–6). Statistically significant differences between PU and NIPUs were computed using one-way ANOVA and Tukey's/Dunnett's multiple comparison testing (*p value ≤ 0.05; ***p value < 0.001).

ting time than the two NIPUs (177 ± 20 s) (p < 0.001). Altogether, our data revealed very low thrombogenicity of NIPUs compared to conventional PU.

2.3 *In vitro* NIPU biocompatibility

In order to assess our NIPU biocompatibility, extracts of PU/NIPU were prepared and added to a monolayer of human primary fibroblasts and human umbilical vein endothelial cells (HUVECs) in culture. Cells were evaluated after these indirect contacts, regarding both their metabolic activity (Fig. 2A and B) and morphology (Fig. 2C and D). Fluorescence measurements based on a resazurin assay revealed mean values of metabolic activity of 78.7 ± 4.5% and 79.6 ± 7.0% after incubation of the fibroblasts with extracts of PPG-NIPU and PTHF-NIPU, respectively. As for fibroblasts in contact with extracts prepared from PU, the mean metabolic activity measured was 78.8 ± 9.6%. No statistically significant difference was found between PU and NIPUs. All percentages were above the threshold (70%) imposed by the ISO standard, confirming the absence of toxic leaching products. Representative confocal microscopy images of the same fibroblasts showed that grown fibroblasts displayed a normal morphology. F-actin stretching and spindle-like shape in all the conditions evaluated corroborated our data on metabolic activity measurements. Similarly, HUVECs showed high metabolic activity in all conditions tested with values of 87.4 ± 5.0%, 93.0 ± 4.1% and 89.5 ± 2.9% after incubation with PPG-NIPU, PTHF-NIPU or PU extracts, respectively. No statistically significant difference was found between PU and NIPUs. HUVECs microscopic observation revealed cells with normal cobblestone appearance

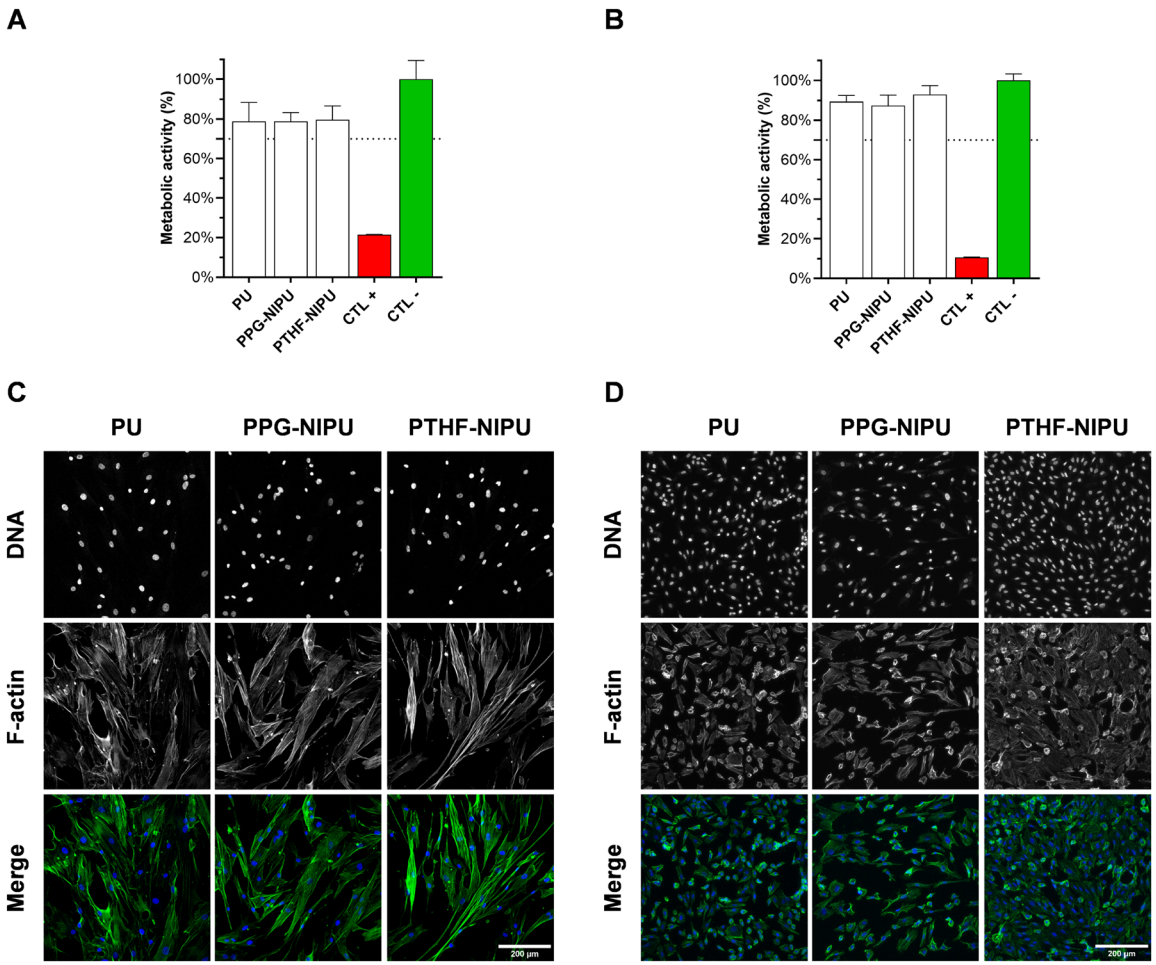

Fig. 2 *In vitro* biocompatibility assessment. (A) Metabolic activity of human fibroblasts after 24 h of indirect contact with PU/NIPU, assessed by a fluorescence resazurin assay. Cells incubated with Triton (X 100) 0.1% (v/v) were used as CTL+, while cells incubated with Dulbecco's modified Eagle's medium (DMEM) alone were used as CTL−. Data are presented as mean with SD (n = 4). Statistically significant differences between PU and NIPUs were not found using one-way ANOVA; (B) metabolic activity of HUVECs after 24 h of indirect contact with PU/NIPU, assessed by a fluorescence resazurin assay. Cells incubated with Triton (X 100) 0.1% (v/v) were used as CTL+, while cells incubated with supplemented endothelial basal medium (EBM-2) alone were used as CTL−. Data are presented as mean with SD (n = 9). Statistically significant differences between PU and NIPUs were not found using one-way ANOVA; (C) fibroblasts nuclei and morphology after 24 h of indirect contact with PU/NIPU. Images represent projections of at least 50 µm height z-stacks. Scale bar: 200 µm; (D) HUVECs nuclei and morphology after 24 h of indirect contact with PU/NIPU. Images represent projections of at least 50 µm height z-stacks. Scale bar: 200 µm.

showing large nuclei. These results demonstrate that NIPUs are not cytotoxic.

2.4 *In silico* valve design definition and NIPU valve manufacturing

Using FSI models of a single leaflet, we first tested 3 different leaflet thickness values (0.3, 0.5 and 0.7 mm), compatible with measurements found for native valves.[38,39] For the 3 thickness values tested (Fig. 3A, B and C) the leaflet fully opened at peak systole and formed a rather circular orifice, allowing a fully centralized flow. However, it was observed that thicker leaflets had a smaller opening area. Indeed, increased thickness resulted in increased maximum orifice velocity: 1.54 m s^{-1} for a 0.3 mm leaflet, 1.84 m s^{-1} for a 0.5 mm leaflet, and 2.39 m s^{-1} for a 0.7 mm leaflet. The radial displacement of the nodule of Arantius (NoA) during the cardiac cycle was also measured: 8.53 mm, 7.73 mm and 6.63 mm for the 0.3 mm, 0.5 mm and 0.7 mm leaflets, respectively. In addition, thicker leaflets dis-

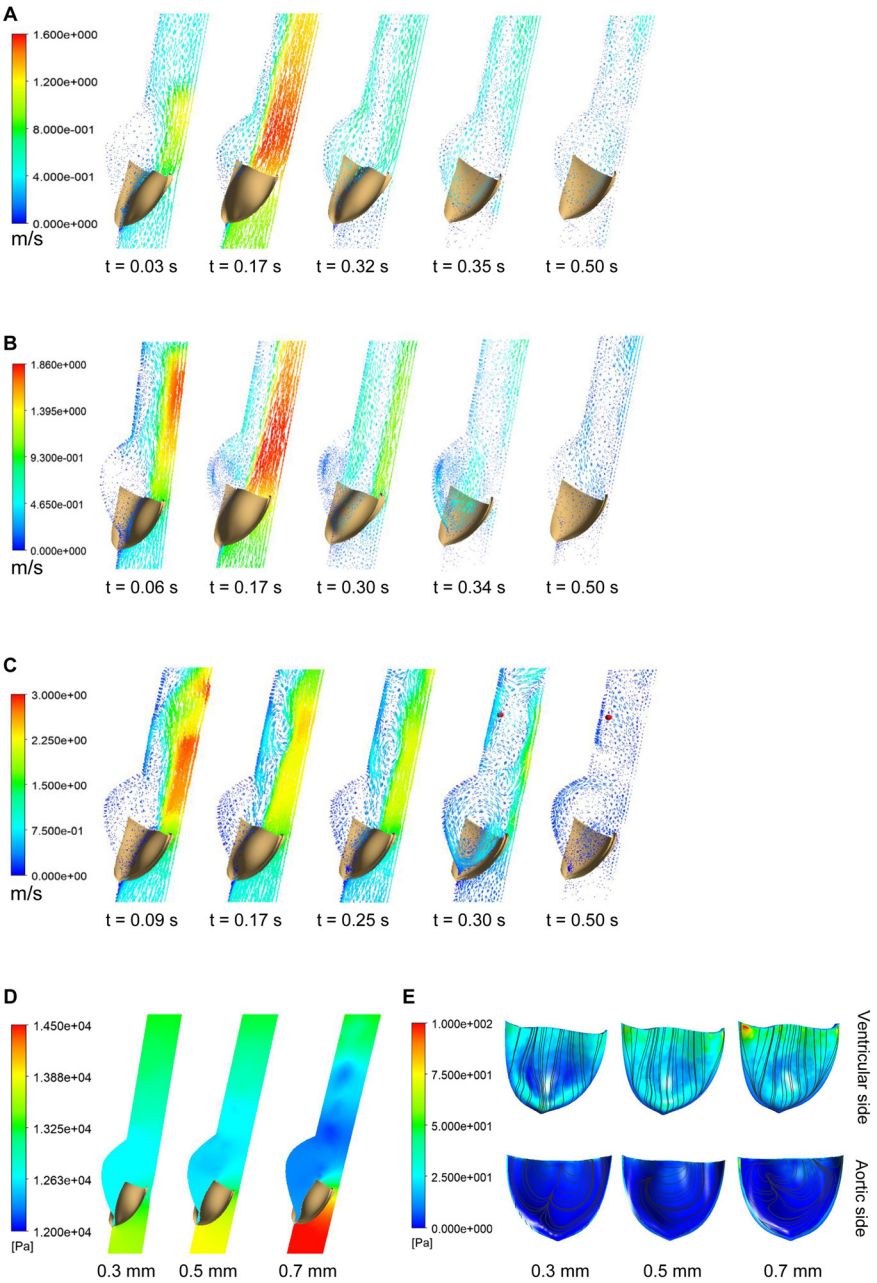

Fig. 3 Velocity vectors, transvalvular pressure gradient and shear stress magnitude for different leaflet thicknesses. Velocity vectors (m s^{-1}) of blood flow at different time points in the cardiac cycle through 0.3 mm (A), 0.5 mm (B) and 0.7 mm (C) leaflets; (D) pressures at peak systole for the 0.3 mm, 0.5 mm and 0.7 mm leaflets; (E) shear stresses and streamlines on the ventricular and aortic sides at peak systole for the 0.3 mm, 0.5 mm and 0.7 mm leaflets.

played a delay in valve opening: 0.3 mm leaflets opened at 0.055 s, while 0.7 mm leaflets opened at 0.1 s. The transvalvular pressure gradient was also calculated and the absolute pressure contours at peak systole are illustrated in Fig. 3D for the 3 thickness values studied. As expected, it was shown that an increase in thickness (meaning a reduction of the opening area) led to an increase of the pressure gradient. The gradient increased from 850 Pa (6.4 mmHg) for the 0.3 mm leaflet to 1200 Pa (9.0 mmHg) (41% increase) for the 0.5 mm leaflet, and further to 2500 Pa (18.8 mmHg) (194% increase) for the 0.7 mm leaflet. Wall shear stress (WSS) is another key parameter which represents the frictional force exerted by the flowing blood on the surface of the leaflets. Shear stress magnitudes at peak systole are shown in Fig. 3E, as well as the streamlines (tangent lines to the shear stress vector field). For all thickness values, the highest shear stresses were found on the leaflets tip. Peaks could be seen near the commissures, with measured values of 47 Pa (0.3 mmHg), 59 Pa (0.4 mmHg) and 100 Pa (0.8 mmHg) for the 0.3 mm, 0.5 mm and 0.7 mm leaflets, respectively. For the next steps of the modeling, a leaflet thickness of 0.5 mm was further used.

We then considered a complete 3D geometry for the next steps of simulation. We performed a 3D scan of the tri-leaflet *Trifecta* bioprosthesis and converted it into a digital mesh as a starting point (design A, Fig. 4A). Design A showed leakage at the commissures, which was reduced in adapted designs B and C. Modelling of the designs A, B and C was initially based on 23 mm diameter valves and details can be found in the ESI (Fig. S8 and S9†). Design B showed the most promising results. FSI model revealed low leakage, geometric orifice area (GOA) of 165.59 mm^2 and maximum velocity of 2.1 m s^{-1}. Design B established a first compromise between reduced leakage and good hydrodynamic performance.

Design B was further improved by fine tuning leaflet size and edges (Fig. 4A). In design B 2.0, the leaflet height was increased, the outer edges of the valve were straightened, and commissure thickness was reduced. Spatial arrangement of the leaflets at peak systole confirmed better opening for design B 2.0 (GOA = 197.05 mm^2). 23 mm diameter valves were then compared to 19 mm diameter valves. For the later, leaflet thickness was adjusted to 0.35 mm and the calculated GOA was 144 mm^2. Velocity vectors at peak systole are shown in Fig. 4B for designs B 23 mm, B 2.0 23 mm, and B 2.0 19 mm. Since the valve orifice area was larger for design B 2.0 23 mm, a slight decrease in velocity was observed when compared to design B 23 mm (maximum drops from 2.1 to 2 m s^{-1}). For design B 2.0 19 mm, 1.93 m s^{-1} was the maximum velocity found. When looking at the radial displacement of the NoA, we observed that design B 2.0 allowed greater opening (maximum NoA displacement of 7.93 mm) than design B (7.25 mm) for 23 mm valves. The maximum NoA displacement for the 19 mm valve was 6.77 mm. Regarding the pressure contours at peak systole (Fig. 4C), transvalvular pressure gradients were 1750 Pa (13.1 mmHg) for design B 23 mm, 1500 Pa (11.3 mmHg) for B 2.0 23 mm, and 1350 Pa (10.1 mmHg) for B 2.0 19 mm. Von-Mises stress and strain distributions at peak systole and diastole for designs B 23 mm, B 2.0 23 mm and B 2.0 19 mm are shown in Fig. 4D. At peak systole, design B 23 mm showed maximum stress and strain values of 0.52 MPa and 17.23%. For design B 2.0 23 mm, 0.57 MPa and 19.07% were found; for design B 2.0 19 mm, maximum stress of 0.58 MPa with maximum strain of 19.18% were measured. However, at peak diastole, the values located near the commissures in design B 23 mm were the highest: Von-Mises stress and strain of 0.76 MPa and 25.48%. For design B 2.0 23 mm, maximum stress was 0.67 MPa (decrease of 12% compared to design B), while the maximum strain was 22.42%. For the 19 mm valve design, Von-Mises stress reached 0.72 MPa, with peak strain of 24.05%. The measurements for design B 2.0 19 mm were slightly higher than for design B 2.0 23 mm, which was expected, considering the reduced thickness of the leaflets. Overall, our results highlighted that design B 2.0 experienced lower stress and strain at peak diastole.

Given the ideal behavior of design B 2.0, a metallic mold was manufactured to produce a NIPU valve by the injection molding technique (Fig. 5). The injection molded valves exhibited well-defined geometry and edges, even though the leaflets displayed unequal thicknesses in some of the produced valves (measurements ranged from 0.35 mm to 0.45 mm).

2.5 Hydrodynamic performance of the valves

NIPU valves were tested in a pulse duplicator to verify that hydrodynamic performance was ISO-compliant. Regurgitation (Fig. 6A), transaortic pressure (Fig. 6B) and effective orifice area (EOA) (Fig. 6C) were measured. NIPU valves were compared to *Mosaic* and *Trifecta* bioprosthetic valves, used in clinics. The mean regurgitation fractions for PPG-NIPU and PTHF-NIPU valves were 4.1 ± 1.9% and 2.9 ± 1.3%, respectively. Similar percentages were obtained for the reference valves: 5.4 ± 0.3% for *Mosaic* and 2.3 ± 0.5% for *Trifecta*. These measurements showed regurgitation values that were lower than the ISO 5840-2:2021 maximum limit of 10%. Regarding transaortic pressure, PPG-NIPU, PTHF-NIPU, and *Mosaic* valves showed values in the same range (34.0 ± 2.5 mmHg, 35.4 ± 2.0 mmHg and 30.6 ± 1.2 mmHg, respectively), while the *Trifecta* experienced lower mean pressure (19.8 ± 0.8 mmHg). Lastly, the valve EOAs were similar for PPG-NIPU, PTHF-NIPU, and *Mosaic* (0.95 ± 0.06 cm^2, 0.85 ± 0.07 cm^2 and 0.99 ± 0.01 cm^2, respectively). *Trifecta* had a larger EOA (1.68 ± 0.02 cm^2) as expected (hence the lower transaortic pressure), given that this bioprosthesis was conceived to increase orifice areas and prevent prosthesis-patient mismatch.[40] Nevertheless, all valves showed mean EOA compliant with ISO 5840-2:2021, that sets a threshold of 0.85 cm^2.

2.6 Absence of calcification after 8 weeks of *in vitro* testing

Because of its superior mechanical properties in the hydrated state, PET-reinforced PTHF-NIPU was the material chosen to proceed with the calcification testing. Patches of PTHF-NIPU and bovine pericardium were placed for 8 weeks in a dynamic

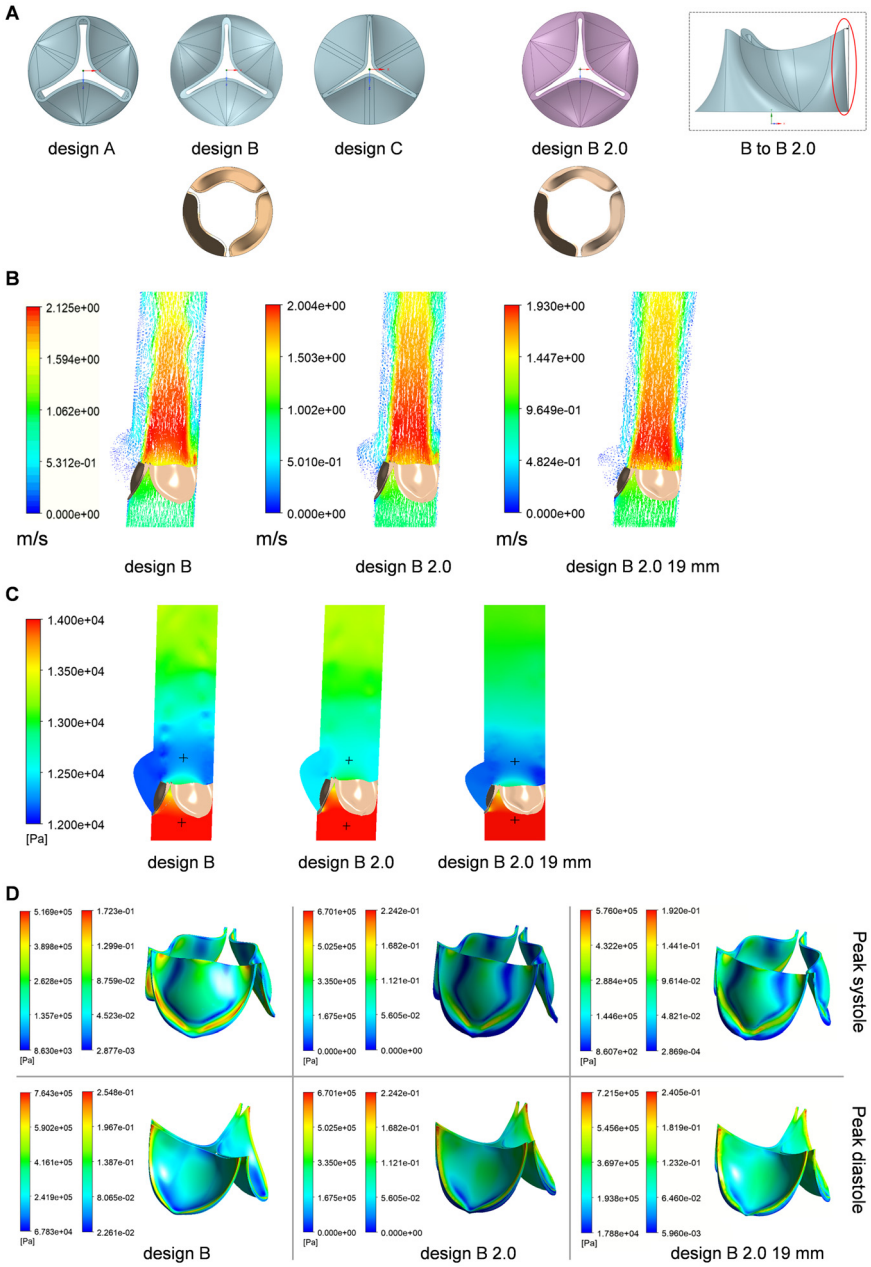

Fig. 4 Comparison between different valve designs. (A) Top view of the initial valve designs A, B and C, as well as the improved version B 2.0 in purple. Detail on the right: to upgrade it, the outer edges of the design B were straightened; (B) comparison between the velocity vectors at peak systole for the designs B 23 mm, B 2.0 23 mm and B 2.0 19 mm; (C) comparison between the pressure gradients at peak systole for the designs B 23 mm, B 2.0 23 mm and B 2.0 19 mm; (D) Von-Mises stress and strain distribution at peak systole and diastole for the designs B 23 mm, B 2.0 23 mm and B 2.0 19 mm.

durability tester in presence of near-physiological and non-spontaneously precipitating fluid, specifically developed for accelerated *in vitro* calcification assessment.[41,42] Calcification was evaluated by measuring ionic concentrations, pH and temperature of the calcification test fluids, and by macro- and microscopic inspection of the patches. The decrease of calcium levels in the fluid of the test compartments was slightly more pronounced for pericardium patches than for NIPUs, although the differences between initial and final concentrations were overall minimal. Changes in the pH or temperature were also negligible (Table 2).

The surface of PTHF-NIPU patches remained smooth and homogeneous with no signs of calcification over the testing period in contrast to pericardium patches that started to calcify from week 5 (Fig. 7). As shown in Fig. 7B, calcium deposits on pericardium patches were often observed in the

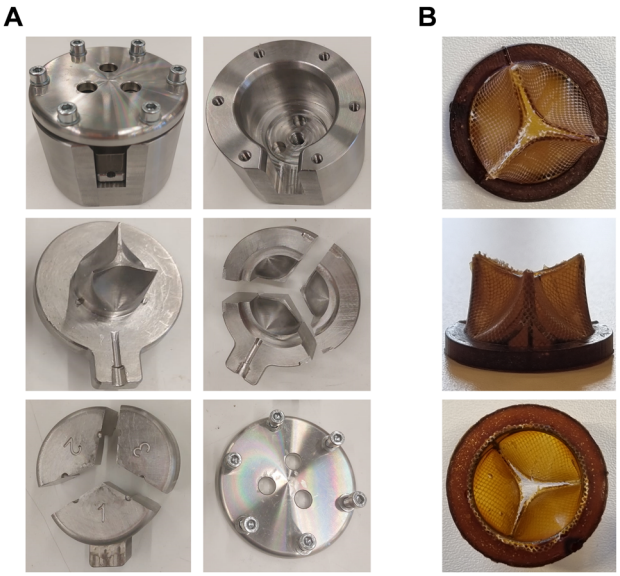

Fig. 5 Mold and NIPU valve. (A) 3D-printed metallic mold (made of stainless steel 316L) and its different parts; (B) top, side and bottom views of a 19 mm (internal diameter) valve produced by injection molding. The insertion of a metallic stent can be observed, as well as the outer support ring.

space between the fixation rings and the patches. These results indicate that PTHF-NIPU are not prone to calcify when compared to bovine pericardium.

3. Discussion

Our work reports the feasibility of using environmentally-friendly NIPU polymers for manufacturing of prosthetic heart valves. First, we succeeded to synthesize two NIPUs that, when reinforced with a PET mesh, showed similar mechanical properties to those of native valve leaflets. We observed that NIPU mechanical properties were altered in hydrated *versus* dry states. In contrast to PU, NIPUs contain hydroxyl (–OH) hydrophilic groups located along the polymer chains that provide strong surface hydration ability[43] by promoting hydrogen bonding with H_2O. The loss of mechanical performance of our NIPUs in the hydrated state may be related to moisture-induced plasticization primarily caused by the presence of those –OH groups, as described for NIPU-based materials.[44–46] A drop in Young's modulus is usually accompanied by a decrease in σ_r, which was observed in our NIPU samples. However, in contrast to Pronoitis *et al.*,[45] an increase in ε_r was not observed neither for PPG-NIPU nor for PTHF-NIPU. The overall mechanical properties of hydrated NIPUs were inferior to the minimal values reported for native leaflets (E = 2 MPa, σ_r = 0.4 MPa, ε_r = 30%).[35,36] Therefore, to limit the impact of swelling on the mechanical performance of the polymers and maintain valve-relevant mechanical characteristics under wet conditions (blood-contacting environment), a PET mesh was successfully incorporated. It is important to highlight that the presence of –OH groups on NIPUs chains offers a broad range of possibilities in terms of functionalization[47] and the attach-

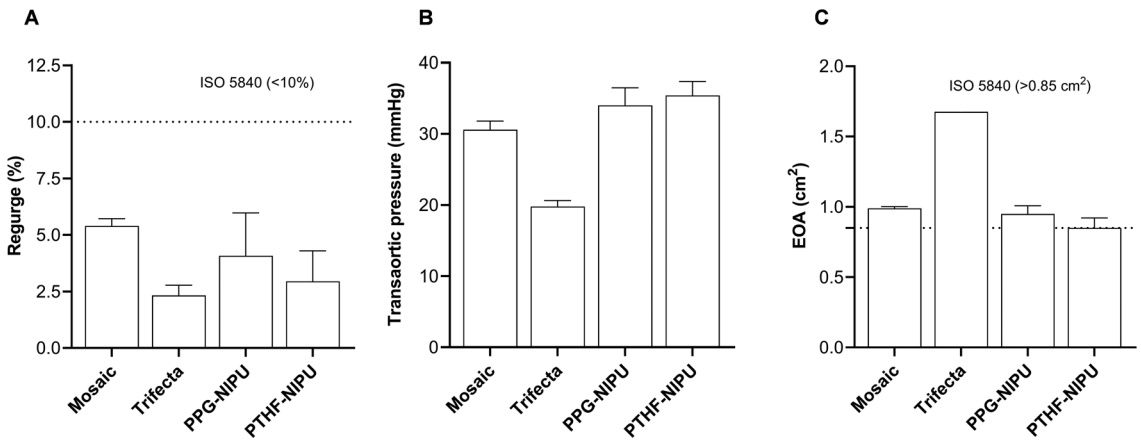

Fig. 6 Hydrodynamic parameters of *Mosaic* and *Trifecta* bioprostheses, PPG-NIPU and PTHF-NIPU valves. (A) Regurgitation fraction; (B) transaortic pressure; (C) effective orifice area (EOA). Parameters were measured in a pulse duplicator with normotensive conditions. Data are presented as mean with SD (n = 2–6).

Table 2 Measurements of initial (week 0) and final (week 8) concentrations of Ca^{2+}, PO_4^{3-}, Na^+ and K^+ (mmol L^{-1}), pH and temperature (°C) of test fluids (mean ± SD, n = 3)

Material	C_i Ca^{2+}	C_f Ca^{2+}	C_i PO_4^{3-}	C_f PO_4^{3-}	C_i Na^+	C_f Na^+	C_i K^+	C_f K^+	pH_i	pH_f	T_i	T_f
PTHF-NIPU	1.9 ± 0.0	1.7 ± 0.1	1.0 ± 0.0	0.9 ± 0.0	141.0 ± 0.0	149.0 ± 3.8	4.7 ± 0.0	5.2 ± 0.1	7.3 ± 0.0	7.3 ± 0.0	35.7 ± 0.1	37.1 ± 0.1
Pericardium	1.9 ± 0.0	1.5 ± 0.1	1.0 ± 0.0	0.8 ± 0.1	141.0 ± 0.0	152.0 ± 7.8	4.7 ± 0.0	5.3 ± 0.3	7.4 ± 0.0	7.3 ± 0.0	34.5 ± 0.1	35.5 ± 0.1

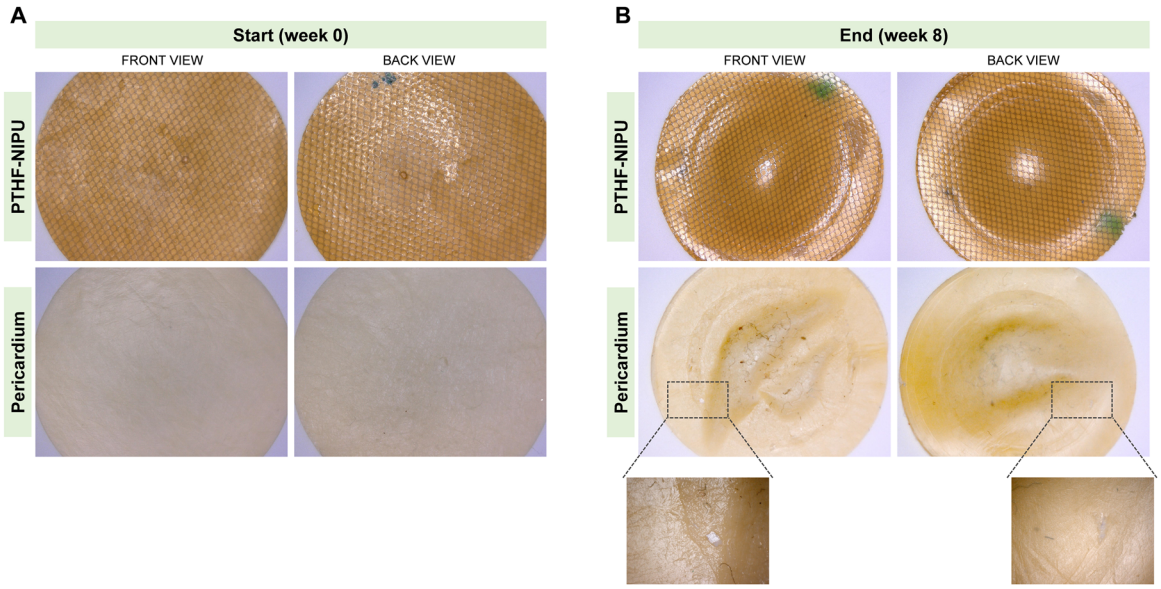

Fig. 7 Macro- and microscopic evaluation of calcification in PTHF-NIPU and pericardium patches. (A) Images of both sides of the patches taken at the starting point (week 0); (B) images of both sides of the patches taken at the end point (week 8). Zoomed areas on pericardium patches show representative examples of deposits.

ment of active biomolecules could eventually play a key role in promoting or inhibiting interesting cell-biomaterial interactions.[48] Checking for polymer degradation in a physiological solution, especially in the context of medical devices or implants, is crucial to ensure the long-term safety and performance of the materials involved. Changes in the material's appearance can be an initial indication of degradation, which can further lead to shifts in thermal properties. In the case of our NIPUs, neither macroscopic alterations nor changes in the original T_gs were observed, suggesting that no degradation occurred during the 14-day testing period.

Secondly, we demonstrate that our NIPU displayed unexpected low thrombogenicity as compared to conventional PU. Thrombosis is the presence of thrombus (blood clots), that will affect blood flow. There are still no studies that fully analyzed NIPUs properties in terms of hemocompatibility and thrombogenicity, although few works describe NIPUs biocompatibility *in vitro*.[49–54] To the best of our knowledge, only three studies reported the interaction of NIPUs of different chemical structures with RBCs. Zhao *et al.*[55] prepared aqueous solutions of non-thermosetting PPG-based NIPU, used as thermoresponsive micelles, and investigated the *in vitro* hemocompatibility of such materials using rabbit blood. NIPU-PBS solutions induced a maximum of 2.8% hemolysis with the most concentrated solution tested. Xu *et al.*[56] observed hemolysis percentages of 1.759% and 3.950% (direct and indirect contacts, respectively) after incubating a fluorescent poly(hydroxyurethane) (FPHU) or its extracts with blood; the materials were therefore slightly hemolytic. Those FPHUs differ from our NIPUs since they were obtained from the reaction of 1,3-bis-(3-glycidoxypropyl) tetramethyldisiloxane and 1,6-hexanediamine. Finally, Gharibi *et al.*[57] prepared a polyurethane-siloxane soybean oil-based coating (also through the non-isocyanate approach) and observed an hemolysis rate of 1.8%. Thus, we synthesized NIPUs that showed lower percentages of hemolysis than previously tested NIPU-based materials (Fig. 1A). So far, studies exploring the interaction of NIPUs with platelets or plasma have not been performed, highlighting the innovative contours of our findings. Our data point to very low levels of platelet adhesion on NIPUs surfaces (Fig. 1B and S7†), which is an important prerequisite for blood-contacting materials, and might mitigate the risk of thrombosis associated with currently available prostheses. Our data also suggested that the synthesized polymers activate less the contact activation system than PU (Fig. 1C). This result represents a unique potential for preventing adverse prosthetic valve-related thrombotic complications.[58] Jaganathan *et al.*[59] showed that PU induced faster coagulation in both prothrombin time (PT) and activated partial thromboplastin time (APTT) tests than modified PUs. This reinforces the idea that pristine PU performs poorly. Considering the general evaluation of *in vitro* hemocompatibility of our NIPUs, these new polymers proved to be non-hemolytic, and they outperform medical-grade PU in terms of platelet adhesion and coagulation activation. It is important to highlight that the PU used as reference is currently the standard material in clinical settings for short and long-term intravenous catheters, which leads to high rates of unsolved thrombotic complications.[60] This emphasizes the potential of exploiting NIPUs remarkable anti-thrombogenic properties for blood-contacting devices like prosthetic valves and beyond.

Regarding cytotoxicity testing of NIPUs, Fanjul-Mosteirín *et al.*[52] have shown that HeLa cells in contact with extracts of hydrogels prepared from polyethylene glycol-based NIPUs dis-

played normal morphology, as well as high metabolic activity. In that study, NIPUs showed a gel-like behavior, suitable for 3D-printed structures for tissue engineering. Similarly, Warner *et al.*[51] confirmed the absence of hazardous leaching solutes of NIPUs obtained from trimethylolpropane allyl ether-cyclocarbonate and 1,5-diaminopentane, observing minimal cell death (3%) after prolonged contact (5 days) of murine myoblasts (C2C12) with NIPU slabs. In that case, NIPUs were 3D-printed with tunable mechanisms *via* click chemistry, generating materials with typically very high Young's moduli, which showed potential to be used when printing rigid structures, different from our elastomers. Our data on *in vitro* biocompatibility of our PPG and PTHF-based NIPU networks (Fig. 2) therefore corroborate previous results on other NIPU-based materials.

In view of very promising features of our newly synthesized NIPUs regarding material properties and *in vitro* hemo/biocompatibility, we then used FSI to conceive an optimal valve design (Fig. 3 and 4). Numerical simulation of the blood flow in the vicinity of a valve indeed offers the possibility to optimize the design in a controlled and specific way.[61] However, numerical simulations on trileaflet valves have received relatively sparse attention in the literature compared to mechanical valves.[8] The goal of our 3D FSI model was to find the optimal valve design before manufacturing our valve prototypes. Velocity fields, transvalvular pressure, wall shear stress, valve opening/closing, and stress/strain on the leaflets were investigated for different valve designs. Von Mises stress takes into account the combined effect of normal and shear stresses, condensing the complex stress state at a point into a single value. This simplification is particularly valuable in the design of components subjected to complex loading conditions, so we considered this parameter more informative than principal stress measurements. Moreover, Von Mises stress, along with fatigue models, allows to estimate the number of cycles a material can endure before failure, which is relevant for our application. The overall hydrodynamic performance of our design B 2.0 was better when compared to design B, with larger opening, lower peak velocity and lower transvalvular pressure. The best hydrodynamic properties (velocity and transvalvular pressure) were obtained for a 19 mm diameter valve with design B 2.0. Modeling and evaluation of aortic valves performance has been developed by several authors using FSI[62–67] while studying the effect of valve shape and geometry on its performance, considering the large deformation of valve leaflets, as well as particular flow characteristics.[39,68] Is has been shown that altering specific angles of a structured stent can significantly lower peak stress on the leaflets, for instance.[66] With the numerical model that our team developed, we could not only find the optimal leaflet thickness, but also the most suitable valve design, reducing stress/strain on the leaflets.

Injection molding was the manufacturing technique used to produce NIPU valves (Fig. 5), allowing cost-effective and more automated production, which represents a paradigm shift given that currently available prostheses still require some degree of manual sewing. The molding technique we explored is relatively simple and easy to scale-up, given that the polymerization of the NIPUs inside the mold is a one-step process. This technique allowed the fabrication of valves with a satisfactory degree of resolution, although slight differences were found in leaflet thicknesses. The micrometer-range variations on the obtained 3D object which depend on temperature and pressure conditions are indeed limitations of the technique. That may impair ideal valve opening, since thickness increase often translates into slower or less efficient opening. More recent advances in materials fabrication (*e.g.* additive manufacturing) may provide opportunities for constructing complex 3D structures with higher precision and even customize them to the patients' needs.[9] However, injection molding offers a solid compromise between production costs, speed and reproducibility.

When performing *in vitro* testing of the produced valves in a pulse duplicator, we were able to comply with ISO standards in terms of hydrodynamic parameters (Fig. 6). Pressures experienced by NIPU valves were slightly higher compared to polymeric valves described in other studies,[69,70] probably due to an asymmetrical opening caused by the unequal leaflet thickness. With this study, we provide a solid starting point for the development of hemodynamically competent NIPU valves, although a long-term evaluation of materials is still needed in the future. Stability of heart valves is an essential feature, knowing that valve prostheses must withstand at least 200 million cycles (equivalent lifetime of 5 years) (ISO standard 5840-2). To be able to conclude on the durability of valves, the testing on a *HiCycle* equipment could be envisioned. Very few studies are available on NIPUs stability, but they are generally described as resistant to chemical degradation[71] and biodegradation.[72] The presence of –OH groups is claimed to enhance the chemical and hydrolytic stability of NIPUs compared to isocyanate-based PUs.[73–75] Further exploring this aspect is certainly part of the future perspectives for our follow-up work on NIPUs.

Calcification (Fig. 7) is one of the main issues of biological valve prostheses, made of porcine or bovine pericardium. This susceptibility of the pericardium to calcify may be associated with the tissue texture conferred by collagen fibers, elastic fibers, glutaraldehyde treatment, debris of dead cells and roughness.[42] Indeed, pericardial valves tend to show calcific deterioration,[76] which leads to valve malfunction and the need for a revision procedure. Efforts to substitute the pericardium-based prosthetic heart valves with polymeric materials date back to the 1960's, although polymer chemists have not yet been able to simultaneously produce an anti-thrombogenic, biocompatible and durable polymeric leaflet substitute.[77] Therefore, the calcification susceptibility of our newly developed NIPUs was evaluated in a new *in vitro* setup,[41,42] where a loss of calcium and phosphate concentration during the test is an indicator for ongoing calcification. Over the 8-week test period, our PTHF-NIPU patches did not calcify. This suggests that the patches had no surface defects, roughness or porosity to the extent necessary to trigger calcification. Contrarily, calci-

fication was observed in the pericardium counterparts, starting at the transition from the firmly clamped to the movable area of the patches where the mechanical bending stress applied to the material was the highest.

Our work opens up new avenues for the development of polymeric valves, although it has some limitations. The first limitation is that PPG-NIPU tends to swell in water over time, which results in altered mechanical performance. The use of PTHF instead of PPG reduced the swelling, but mechanical properties had to be improved by incorporation of a PET mesh. The need to incorporate PET to reinforce NIPU networks represents a clear disadvantage compared to PU, which exhibits good mechanical performance by default. Pristine NIPUs were also less performant than native tissues, although an improvement was observed after PET incorporation. Another drawback lays on the fact that studies on delamination on the surface of NIPUs are missing, as these phenomena are known to occur *in vivo*, leading to material degradation. It will therefore be essential to further explore the susceptibility of the polymer networks to delaminate, especially in the presence of blood. Regarding the FSI model developed by us, it would have been interesting to also test a nonlinear hyperelastic model, to compare its accuracy in predicting the behavior of NIPU elastomers. Regarding valve manufacturing, the incorporation of a PET mesh may increase surface roughness, which could affect the interaction with blood components. The valve manufacturing technique chosen (injection molding) led to the production of leaflets with unequal thickness, which impaired optimal valve opening, particularly on PTHF-NIPU valves, that displayed a mean EOA that corresponds to the limit imposed by the ISO standard. Lastly, valve durability should be assessed in a durability tester mimicking the mechanical challenge imposed to a cardiac valve over the years in future perspectives of this work.

4. Conclusion

New NIPU elastomer networks were successfully obtained by mixing bis(cyclic carbonate) polyethers with a diamine and a triamine. PPG-NIPU and PTHF-NIPU displayed interesting properties, compatible with a potential use as prosthetic heart valve materials. These NIPUs not only represent the "green" alternative to PU, but they also showed an extremely low thrombogenic profile. A 3D FSI computational model was developed to study different valve designs and behaviors at peak systole/diastole, and revealed efficiency in predicting real valve performances. A metallic mold was produced according to the defined design, and NIPU valves were obtained by injection molding. Testing of the NIPU valves in a pulse duplicator showed good hydrodynamic performance. The verification that computational modeling results translate into *in vitro* compliance can also lead to customizable patient-specific valve design. Resistance to calcification was observed for PTHF-NIPU patches. Our study sets up the basis for future development of isocyanate-free, hemocompatible and hydrodynamically competent prosthetic heart valves made of NIPU.

5. Experimental section

5.1 Synthesis of precursors and polymers

Synthesis of poly(propylene glycol) bis(cyclic carbonate). Poly(propylene glycol) bis(cyclic carbonate) (PPG bisCC) was prepared according to Bähr and Mülhaupt's protocol[78] by the catalyzed coupling of CO_2 to epoxides. Briefly, poly(propylene glycol) diglycidyl ether (PPG DE, 380 g mol^{-1}, 1 equivalent) and tetrabutylammonium iodide (TBAI, catalyst, 0.05 equivalent) were introduced in a 80 mL stainless-steel high pressure autoclave, which was then filled with 100 bar of CO_2 and heated up to 80 °C. The reaction was kept at constant pressure for 24 h to reach complete conversion. After depressurization of the reactor, the product was collected and TBAI was removed by three liquid–liquid extractions. ^{1}H-nuclear magnetic resonance (NMR) spectra are shown in Fig. S1A† and confirm the previously reported PPG bisCC structure.[79]

Synthesis of poly(tetrahydrofuran) di-epoxide and bis(cyclic carbonate). Poly(tetrahydrofuran) di-epoxide (PTHF DE) was synthesized from the epoxidation of commercial PTHF (650 g mol^{-1}) using epichlorohydrin. Briefly, 30 g of PTHF were dissolved in 150 mL of anhydrous toluene and dried by azeotropic distillation of the solvent (3×). After that, sodium hydride (3.32 g) was used to allow the conversion of the hydroxy end groups of PTHF into sodium alkoxide. An excess of non-distilled epichlorohydrin (4 equivalent) was added to the mixture and reacted for 48 h at 40 °C. Fig. S1B† shows the ^{1}H-NMR spectra of PTHF DE in deuterated chloroform, confirming successful epoxidation. The synthesized PTHF DE (1 equivalent), together with tetrabutylammonium bromide (TBAB, catalyst, 0.1 equivalent), were then introduced in a 80 mL high pressure autoclave to synthesize PTHF bisCC, following the same procedure and reaction conditions as those described above for the production of PPG bisCC. PTHF bisCC was purified by precipitation in water. Fig. S1B† shows the ^{1}H-NMR spectra of PTHF bisCC in deuterated chloroform, confirming complete conversion.

Synthesis of non-isocyanate polyurethane (NIPU) networks. Either PPG bisCC (468 g mol^{-1}, 1 equivalent) or PTHF bisCC (850 g mol^{-1}, 1 equivalent) was mixed with 4-((4-aminocyclohexyl)methyl)-cyclohexanamine (MBCHA, 0.2 equivalent) and *N*′,*N*′-bis(2-aminoethyl)ethane-1,2-diamine (TAEA, 0.53 equivalent), and magnetically stirred in bulk at 40 °C for 15 min. Based on previously described procedures,[79] no catalyst was used. The solutions were then poured into a flat Teflon mold (0.5 × 5 × 25 mm) and thermally cured in an oven at 70 °C for 24 h. PPG-NIPU and PTHF-NIPU polymer cross-linked networks were obtained.

5.2 Characterization methods

Nuclear magnetic resonance spectroscopy (NMR). Samples were prepared by dissolving 20 mg of each product in 700 µl of

deuterated chloroform ($CDCl_3$). ^{1}H-NMR spectra were recorded at 298 K with a Bruker advance DRX 400 MHz spectrometer, in the Fourier transform (FT) mode.

Differential scanning calorimetry (DSC). Glass-transition temperatures (T_g) were determined with TA Instruments DSC Q100 thermal analyzer. Data were analyzed with TA Instruments Universal Analysis 2000 software. The following procedure was used: equilibrium at −60 °C and isothermal step of 2 min (first cycle); heating ramp of 10 °C min^{-1} up to 120 °C followed by an isothermal step of 2 min (second cycle); equilibrium at −60 °C and isothermal step of 2 min (third cycle); heating ramp of 10 °C min^{-1} up to 200 °C (fourth cycle). T_g was measured at the inflection point of the curves.

Contact angle. Contact angles were measured using a DGD Fast/60 equipment with the software WINDROP by GBX Instruments. For each measurement, a droplet of 15 μL of Milli-Q water was placed on the NIPU surface. Contact angles between the surfaces and the droplet's tangent were then determined after 180 seconds.

Water uptake and mechanical properties. The equilibrium water absorption (EWA) of NIPUs was determined by accurately weighing the samples first in dried state (W_d) and then in wet state (W_s), obtained upon soaking in water at room temperature (RT) for 24 h. EWA percentages were calculated using the following equation: EWA (%) = $((W_s - W_d)/W_d) \times 100$. Expansion (%) of the samples in every direction was calculated by measuring the sample dimensions (thickness/width/length) first in dried state and then after one week in phosphate buffered saline (PBS). The elastic modulus (E), the ultimate tensile strength (σ_r) and the fracture strain (ε_r) of the samples were measured at RT using a tensile testing equipment (Instron 5566) with a force speed of 0.05 MPa min^{-1}. Samples were analyzed in dried state (after drying at 100 °C) and wet state (after immersion in water for 24 h).

Degradation and stability over time. Degradation of the polymers was investigated through long-term soak testing, incubating the NIPU discs with PBS at 37 °C under mild agitation (100 rpm) for 14 days. The pH of the buffer was measured at day 0 and day 14 using a Fisherbrand™ accumet™ AE150 benchtop pH meter. Regarding the NIPU discs, a visual inspection of the material was the first step, to look for signs of discoloration, cracking or surface changes. After that, the materials were analyzed by DSC to verify that they had maintained original thermal properties, particularly T_g values.

5.3 *In vitro* hemocompatibility assessment

The study on blood samples from healthy human volunteers was conducted upon approval by our institutional ethical committee (Reference 2015/69, B707201524356) in accordance with European legal requirements and the revised Helsinki declaration. All donors signed an informed consent. In all *in vitro* hemocompatibility tests, medical-grade Carbothane™ was used as reference material. Carbothane™ is an aliphatic PCU. Polymers bearing PCU moieties were already tested for valves[20,24,25] and are used for short and long-term blood-contacting catheters. Carbothane™ PU, as well as the synthesized polymers (PPG-NIPU and PTHF-NIPU), were cut into 5 mm diameter discs (Fig. S2†). These discs were rinsed with NaCl 0.9% (w/v) for 72 h (refreshing the NaCl solution every day) at 37 °C under mild agitation (100 rpm), and sterilized under UV (15 minutes of exposure each side).

Hemolysis. *In vitro* hemocompatibility was firstly evaluated through hemolysis testing with human red blood cells (RBCs). Blood was collected by venipuncture into citrated tubes (3.2% sodium citrate). The first 3 mL were discarded to avoid tissue factor effects. Blood samples were centrifuged at 150*g* for 15 min and platelet-rich plasma (PRP) was removed. RBCs were resuspended in PBS and centrifuged at 800*g* for 10 min. RBCs were washed twice in PBS, or until the supernatant was clear. A solution of 1 : 7 RBCs/PBS was used for the test samples, as well as for the negative control. A solution of 1 : 7 RBCs/distilled water (dH_2O) was used as positive control of hemolysis. PU/NIPUs were incubated with 1 : 7 RBCs/PBS for 3 h at 37 °C on an orbital shaker at 100 rpm. Surface-area-to-volume ratios complied with ISO 10993-4:2017 and ASTM Standard F756-00. After 3 h, the RBCs solutions incubated with the polymers, as well as the controls, were centrifuged at 800xg for 15 min, the supernatants were transferred to a 96-well plate (Greiner CELLSTAR®), and the absorbance was measured ($\lambda \approx 545$ nm) using a micro-plate reader. Absorbance values were compared to positive and negative controls, and hemolysis rates were displayed in percentage. Statistically significant differences between PU and NIPUs were calculated through one-way ANOVA with Tukey's multiple comparisons test.

Platelet adhesion: lactate dehydrogenase activity. Citrated blood was centrifuged at 150*g* for 15 min, PRP was collected and platelets were counted. Platelet density was adjusted to 250 000 platelets per μL with autologous platelet-poor plasma (PPP). PU and the synthesized NIPUs were incubated with PRP (each disc with a volume of 130 μL) in Eppendorf tubes for 2 h at 37 °C on an orbital shaker at 100 rpm. After 2 h of incubation, the polymer discs were rinsed with PBS and adherent platelets were subsequently lysed with 100 μL of Triton (X-100) 1% (v/v) for 5 min while pipetting up and down. The lysates were transferred to a 96-well plate (Greiner CELLSTAR®) and lactate dehydrogenase (LDH) activity in the lysates was measured using a colorimetric assay kit from Sigma-Aldrich. Absorbance values ($\lambda \approx 450$ nm) were compared to positive and negative controls (provided with the commercial kit), and statistically significant differences between PU and NIPUs were calculated through one-way ANOVA with Dunnett's multiple comparisons test.

Platelet adhesion: flow experiments. Platelet adhesion was also assessed under flow according to De Witt *et al.*[37] Briefly, glass coverslips were coated for 1 h with 2 microspots (1 μL) of chloroform-dissolved medical grade PU or linear NIPUs. After a 30 min blocking step with bovine serum albumin, coverslips were mounted in a parallel plate flow chamber. Citrated blood was supplemented with 3,3′-dihexyloxacarbocyanine iodide (0.5 μg mL^{-1}) to label the platelets and recalcified in the presence of D-phenylalanyl-L-prolyl-L-arginine chloromethyl ketone

(40 μM) just prior to perfusion at a wall shear rate of 1000 s^{-1} for 3.5 min. Brightfield and fluorescence images were captured using an EVOS microscope (Bothel). Microscopic images were analyzed using specific scripts[37,80] written with the open-access Fiji-ImageJ software (Laboratory for Optical and Computational Instrumentation, University of Wisconsin–Madison). Surface area coverage (SAC) of adhered platelets was then determined from fluorescent images.

Coagulation activation. Human pooled PPP (CRYOcheck) was thawed at 37 °C for 5 min. PU/NIPU discs were incubated with 130 μL of PPP in Eppendorf tubes for 2 h at 37 °C on an orbital shaker at 100 rpm. PPP alone was used as negative control of coagulation activation, while kaolin-coated glass coverslips were used as positive control. After 2 h of incubation, clotting time was measured by using a non-activated partial thromboplastin time (NaPTT) test. NaPTT reagent (NODIA) (50 μL) was added to 50 μL of the PPP samples in a plastic single-use cuvette and incubated for 1 min at 37 °C. A magnetic bead was inserted in the cuvette, a solution of calcium chloride (0.025 M, 50 μL) was then added to the pre-warmed samples, and clotting endpoints were measured with a STart4 apparatus. Statistically significant differences between PU and NIPUs were calculated through one-way ANOVA with Dunnett's multiple comparisons test.

5.4 *In vitro* biocompatibility assessment

In all *in vitro* biocompatibility tests, the medical-grade Carbothane™ PU described above was used as reference material. Carbothane™ PU, as well as the synthesized polymers (PPG-NIPU and PTHF-NIPU), were cut into 5 mm diameter discs (Fig. S2†). These discs were rinsed with NaCl 0.9% (w/v) for 72 h (refreshing the NaCl solution every day) at 37 °C under mild agitation (100 rpm), and sterilized under UV (15 minutes of exposure each side).

Primary cells and culture conditions. *In vitro* biocompatibility assays were performed using primary cultures of human dermal fibroblasts (HDFa ATCC PCS-201-012) and human umbilical vein endothelial cells (HUVEC ATCC PCS-100-010). Fibroblasts were cultured in Dulbecco's modified Eagle's medium (DMEM) supplemented with 10% (v/v) fetal bovine serum (FBS), 1% (v/v) non-essential amino acids (NEAA), 2.5 μg mL^{-1} of amphotericin B and 1% (v/v) penicillin/streptomycin. HUVECs were grown in endothelial cell growth basal medium (EBMTM-2) supplemented with the EGMTM-2 SingleQuots™ kit. Cells were incubated at 37 °C, in a humidified atmosphere, containing 5% CO_2. Medium was refreshed every two days.

Indirect contact. The cytocompatibility of the synthesized NIPUs was evaluated using an indirect contact assay, by incubating the human fibroblasts and HUVECs with extracts of the materials, prepared as described in ISO 10993-12:2021. Briefly, 5 mm polymer discs, previously washed and sterilized as described above, were incubated with cell culture medium (DMEM or EBMTM-2 depending on the cell type) in Eppendorf tubes for 24 h at 37 °C on an orbital shaker at 100 rpm (4 discs/500 μL). Cells were seeded in 96-well plates (Greiner CELLSTAR®) at a density of 1×10^5 cells per mL and kept in culture for 24 h before adding PU/NIPU extracts (100 μL to each well) for additional 24 h, according to ISO 10993-5:2009. Cells incubated with DMEM/EBMTM-2 alone were used as negative control and cells incubated with Triton (X-100) 0.1% (v/v) were used as positive control.

Measurement of the metabolic activity. Metabolic activity of the fibroblasts/HUVECs after 24 h of exposure to materials extracts was quantified using a resazurin-based assay. For all tested conditions (extracts and controls), cells were incubated in medium containing 10% (v/v) resazurin for 4 h. Afterwards, medium (100 μL) was transferred to a black 96-well plate with clear bottom (Corning®) and relative fluorescence units (RFUs) were measured ($\lambda_{ex} \approx 530$ nm, $\lambda_{em} \approx 590$ nm) using a microplate reader. RFU values were compared to positive and negative controls, and metabolic rates were displayed in percentage. Statistically significant differences between PU and NIPUs were calculated through one-way ANOVA with Dunnett's multiple comparisons test.

Visualization of adherent cells. After 24 h of incubation with PU/NIPU extracts, fibroblasts/HUVECs were rinsed with PBS (100 μL), fixed with 100 μL of paraformaldehyde (PFA) 4% (w/v) in PBS, washed 3 times with PBS, and prepared for visualization by fluorescent confocal microscopy. For that, cells were permeabilized with Triton (X-100) 0.1% (v/v), washed 3 times with PBS, and stained for the identification of deoxyribonucleic acid (DNA) and filamentous actin (F-actin), using 6-diamidino-2-phenylindole dihydrochloride (DAPI) (3 μg mL^{-1}), and phalloidin conjugated with Alexa Fluor 488 (1 : 100 dilution), respectively. Representative scanned *z*-series of the samples were imaged using a confocal microscope (Nikon A1R), and the acquired *z*-stacks were projected onto a single plane and pseudo-colored using Fiji-ImageJ software.

5.5 Fluid-structure interaction (FSI), mold and valve manufacturing

Computational modeling. A 3D fluid-structure interaction (FSI) computational model was developed to predict aortic valve hydrodynamics and define the optimal valve design. All parameters were computed with the Multiphysics Simulation Software Ansys 19.0 (ANSYS, Inc., Canonsburg, PA, USA). Our model considered the interaction between the valve and the surrounding blood by incorporating both fluid dynamics and valve structural responses (2-way approach). The numerical model included the aortic root with three hemispherical enlargements representing the sinuses of Valsalva and the valve with three thin, flexible leaflets. The Young's moduli of NIPUs reinforced with poly(ethylene terephthalate) (PET) were considered for the FSI modeling (a value of 3 MPa was used, since both PPG-NIPU + PET and PTHF-NIPU + PET showed measurements of $E > 3$ MPa in the hydrated state – see Results section 1). Other properties were used to describe the stiffness of the materials, considering the generalized Hooke's law: Poisson's ratio, bulk modulus and shear modulus values of 0.35, 3.33 MPa and 1.11 MPa, respectively. The density of the NIPUs was determined to be 1900 kg m^{-3}. Detailed methods regarding

the coupling approach, model geometry, structural/fluid domains and boundary conditions, and spatial discretization – meshing – can be found in ESI,† particularly illustrated in Fig. S3, S4, S5 and S6,† respectively. Our starting valve design was built from the 3D scan of a *Trifecta* bioprosthesis converted to a digital mesh. The polymeric valve was modelled as a homogeneous isotropic material. Blood was modelled as an incompressible Newtonian fluid[61,81] with density (ρ) of 1060 kg m^{-3} (ref. 82) and constant dynamic viscosity coefficient (μ) of 0.004 (kg m^{-1}) s^{-1}. The flow was assumed as laminar.

Mold and injection molding. A computer-aided design (CAD) file was generated and a metallic mold was manufactured, matching defined valve design. Stainless steel 316L was used to prevent rusting and corrosion, undesired side reactions with the material, or biocompatibility issues arising therefrom. Injection molding was used to produce the valves, which consisted of injecting the polymer in its liquid form into the mold, and allowing it to cross-link and solidify at high temperature (24 h in the oven at 70 °C). Before proceeding to polymer injection, a PET mesh (Dacron 3002, Surgical Mesh™) was added in the mold to increase mechanical resistance of manufactured valves. In addition, a metallic support was produced to maintain valve structure. After crosslinking in a solid network, the polymers were demolded, and valves with a well-defined geometry were obtained.

5.6 Hydrodynamic performance of the valves

Manufactured tri-leaflet NIPU valves with an internal diameter of 19 mm (this diameter was preferred because of its suitability for future *in vivo* preclinical testing in sheep) were placed in the aortic valve position of a left heart model (pulse duplicator equipment, from *ViVitro labs*). Regurgitation fraction, transaortic pressure and effective orifice area (EOA) were measured under normotensive conditions (70 beats min^{-1}; cardiac output of 5 L min^{-1}), following the indications in the ISO 5840-1:2021. NIPU valves were compared with *Mosaic* (internal diameter of 18.5 mm, Medtronic) and *Trifecta* (internal diameter of 19 mm, Abbott), both bioprosthetic valves currently used in clinics.

5.7 *In vitro* calcification assessment

Accelerated material calcification was tested over 8 weeks using a heart valve durability tester CVE-FT2 and a specially designed calcification fluid.[42] Calcification tests allowed to evaluate calcium deposits on synthesized PTHF-NIPU and commercial St Jude Medical (SJM) bovine pericardium patches, through microscopic analysis and measurements of ionic concentrations. Briefly, calcification fluid was produced and all samples were microscopically evaluated before the start of the test. To initiate the tester, patches were clamped between rigid polyvinyl chloride (PVC) fixation rings with an outer diameter of 38 mm and an inner diameter of 16 mm and mounted into separate test compartments. Calcification fluid at physiological temperature of 37 °C and a pH value of 7.4 was transferred into the compartments and test frequency was adjusted to 300 bpm. According to ISO 5840, patches were loaded with a peak differential pressure of 100 mmHg. The pressure was controlled every 2 days and the calcification fluid replenished every 7 days. After a total of 8 weeks, the tester was stopped, and the samples were demounted and observed by microscopic analysis. Additionally, the fluid's ionic concentrations were analyzed.

Author contributions

S. F. Melo: Conceptualization, methodology, validation, formal analysis, investigation, writing – original draft. A. Nondonfaz: Methodology, software, formal analysis, investigation. A. Aqil: Conceptualization, methodology, investigation. A. Pierrard: Conceptualization, methodology, investigation. A. Hulin: Conceptualization, methodology, investigation. C. Delierneux: Conceptualization, project administration. B. Ditkowski: Methodology, project administration. M. Gustin: Conceptualization, investigation. M. Legrand: Methodology, investigation. B. M. E. Tullemans: Methodology, investigation. S. L. N. Brouns: Methodology, investigation. A. Nchimi: Conceptualization. R. Carrus: Conceptualization. A. Dejosé: Conceptualization. J. W. M. Heemskerk: Conceptualization, methodology. M. J. E. Kuijpers: Conceptualization, methodology. J. Ritter: Methodology, investigation. U. Steinseifer: Conceptualization, methodology. J. C. Clauser: Conceptualization, methodology. C. Jérôme: Conceptualization, supervision. P. Lancellotti: Conceptualization, supervision. C. Oury: Conceptualization, writing – review & editing, supervision.

Conflicts of interest

There are no conflicts of interest to declare.

Acknowledgements

Authors would like to acknowledge the funding from the Cooperation Program Interreg V-Euregio Meuse Rhin (European Commission) in the frame of the PolyValve project; the Fonds de la Recherche Scientifique (F. R. S.-FNRS, Belgium) in the frame of the FRIA grant attributed to S. F. Melo, and the Research Director position of C. Oury. S. F. Melo obtained additional financial support from the GIGA Doctoral School for Health Sciences and the Fondation Léon Fredericq (Belgium).

References

1 A. Timmis, P. Vardas, N. Townsend, A. Torbica, H. Katus, D. De Smedt, C. P. Gale, A. P. Maggioni, S. E. Petersen, R. Huculeci, *et al.*, *Eur. Heart J.*, 2022, **43**, 716.
2 C. W. Tsao, A. W. Aday, Z. I. Almarzooq, A. Alonso, A. Z. Beaton, M. S. Bittencourt, A. K. Boehme, A. E. Buxton, A.

P. Carson, Y. Commodore-Mensah, *et al.*, *Circulation*, 2022, **145**, E153.
3 L. J. Davidson and C. J. Davidson, *J. Am. Med. Assoc.*, 2021, **325**, 2480.
4 C. W. Tsao, A. W. Aday, Z. I. Almarzooq, A. Alonso, A. Z. Beaton, M. S. Bittencourt, A. K. Boehme, A. E. Buxton, A. P.Carson, Y. Commodore-Mensah, M. S. V. Elkind, K. R. Evenson, C. Eze-Nliam, J. F. Ferguson, G. Generoso, J. E. Ho, R. Kalani, S. S. Khan, B. M. Kissela, K. L. Knutson, D. A. Levine, T. T. Lewis, J. Liu, M. S. Loop, J. Ma, M. E. Mussolino, S. D. Navaneethan, A. M. Perak, R. Poudel, M. Rezk-Hanna, G. A. Roth, E. B. Schroeder, S. H. Shah, E. L. Thacker, L. B. VanWagner, S. S. Virani, J. H. Voecks, N. Y. Wang, K. Yaffe and S. S. Martin, *Circulation*, 2022, **145**(8), e153–e639, (DOI: **10.1161/CIR.0000000000001052**, Epub 2022 Jan 26. Erratum in: *Circulation*. 2022 Sep 6;146(10):e141. PMID: 35078371.).
5 A. E. Kostyunin, A. E. Yuzhalin, M. A. Rezvova, E. A. Ovcharenko, T. V. Glushkova and A. G. Kutikhin, *J. Am. Heart Assoc.*, 2020, **9**(19), e018506.
6 C. M. Otto, R. A. Nishimura, R. O. Bonow, B. A. Carabello, J. P. Erwin, F. Gentile, H. Jneid, E. V. Krieger, M. Mack, C. McLeod, *et al.*, *J. Am. Coll. Cardiol.*, 2021, **77**, e25.
7 M. A. Rezvova, K. Y. Klyshnikov, A. A. Gritskevich and E. A. Ovcharenko, *Int. J. Mol. Sci.*, 2023, **24**, DOI: **10.3390/ijms24043963**.
8 T. E. Claiborne, M. J. Slepian, S. Hossainy and D. Bluestein, *Expert Rev. Med. Devices*, 2012, **9**, 577.
9 F. Oveissi, S. Naficy, A. Lee, D. S. Winlaw and F. Dehghani, *Mater. Today Bio*, 2020, **5**, 100038.
10 M. Crago, A. Lee, S. Farajikhah, F. Oveissi, D. F. Fletcher, F. Dehghani, D. S. Winlaw and S. Naficy, *Mater. Today Commun.*, 2022, 104916.
11 K. Navas-Gómez and M. F. Valero, *Materials*, 2020, **13**(15), DOI: **10.3390/ma13153250**.
12 R. L. Li, J. Russ, C. Paschalides, G. Ferrari, H. Waisman, J. W. Kysar and D. Kalfa, *Biomaterials*, 2019, **225**, 119493.
13 J. Jansen and H. Reul, *J. Med. Eng. Technol.*, 1992, **16**, 27.
14 J. Jansen, S. Willeke, B. Reiners, P. Harbott, H. Reul, H. B. Lo, S. Däbritz, C. Rosenbaum, A. Bitter and K. Ziehe, *ASAIO Trans.*, 1991, **37**, M451.
15 T. G. Mackay, G. M. Bernacca, A. C. Fisher, C. S. Hindle and D. J. Wheatley, *Artif. Organs*, 1996, **20**, 1017.
16 G. M. Bernacca, T. G. Mackay, R. Wilkinson and D. J. Wheatley, *Biomaterials*, 1995, **16**(4), 279–285.
17 G. M. Bernacca and D. J. Wheatley, *Int. J. Artif. Organs*, 1998, **21**, 814.
18 G. M. Bernacca, T. G. Mackay, M. J. Gulbransen, A. W. Donn and D. J. Wheatley, *Int. J. Artif. Organs*, 1997, **20**, 327.
19 S. L. Hilbert, V. J. Ferrans, Y. Tomita, E. E. Eidbo and M. Jones, *J. Thorac. Cardiovasc. Surg.*, 1987, **94**, 419.
20 S. H. Daebritz, B. Fausten, B. Hermanns, A. Franke, J. Schroeder, J. Groetzner, R. Autschbach, B. J. Messmer and J. S. Sachweh, *Heart Surg. Forum*, 2004, **7**, 371.
21 D. J. Wheatley, G. M. Bernacca, M. M. Tolland, B. O'connor, J. Fisher and D. F. Williams, *Int. J. Artif. Organs*, 2001, **24**, 95.
22 D. J. Wheatley, L. Raco, G. M. Bernacca, I. Sim, P. R. Belcher and J. S. Boyd, *European Journal of Cardio-Thoracic Surgery*, 2000, **17**(4), 440–448.
23 G. M. Bernacca, B. O'Connor, D. F. Williams and D. J. Wheatley, *Biomaterials*, 2002, **23**, 45.
24 S. K. Singh, M. Kachel, E. Castillero, Y. Xue, D. Kalfa, G. Ferrari and I. George, *Front. Cardiovasc. Med.*, 2023, 10.
25 S. H. Daebritz, J. S. Sachweh, B. Hermanns, B. Fausten, A. Franke, J. Groetzner, B. Klosterhalfen and B. J. Messmer, *Circulation*, 2003, **108**, 134–139.
26 A. G. Kidane, G. Burriesci, M. Edirisinghe, H. Ghanbari, P. Bonhoeffer and A. M. Seifalian, *Acta Biomater.*, 2009, **5**, 2409.
27 R. Y. Kanna, H. J. Salacinski, J. De Groot, I. Clatworthy, L. Bozec, M. Horton, P. E. Butler and A. M. Seifalian, *Biomacromolecules*, 2006, **7**, 215.
28 B. Rahmani, S. Tzamtzis, R. Sheridan, M. J. Mullen, J. Yap, A. M. Seifalian and G. Burriesci, *J. Cardiovasc. Transl. Res.*, 2017, **10**(2), 104.
29 E. A. Ovcharenko, A. Seifalian, M. A. Rezvova, K. Yu Klyshnikov, T. V. Glushkova, T. Akenteva, L. V. Antonova, E. A. Velikanova, V. S. Chernonosova, G. Yu Shevelev, *et al.*, *Sci. Rep.*, 2020, (10), 5271.
30 A. Cavallo, E. Gasparotti, P. Losi, I. Foffa, T. Al Kayal, E. Vignali, S. Celi and G. Soldani, *J. Mech. Behav. Biomed. Mater.*, 2021, **115**, DOI: **10.1016/J.JMBBM.2020.104294**.
31 Foldax, "Home | Tria Valve by Foldax", can be found under **https://foldax.com/**, **nd**.
32 P. Stachak, I. Łukaszewska, E. Hebda and K. Pielichowski, *Materials*, 2021, **14**(13), 3497.
33 A. Gomez-Lopez, F. Elizalde, I. I. Calvo and H. Sardon, *Chem. Commun.*, 2021, **57**, 12254.
34 S. Wendels and L. Avérous, *Bioact. Mater.*, 2021, **6**, 1083.
35 A. Hasan, K. Ragaert, W. Swieszkowski, Š. Selimović, A. Paul, G. Camci-Unal, M. R. K. Mofrad and A. Khademhosseini, *J. Biomech.*, 2014, **47**, 1949.
36 A. Balguid, M. P. Rubbens, A. Mol, R. A. Bank, A. J. J. C. Bogers, J. P. Van Kats, B. A. J. M. De Mol, F. P. T. Baaijens and C. V. C. Bouten, *Tissue Eng.*, 2007, **13**, 1501.
37 S. M. De Witt, F. Swieringa, R. Cavill, M. M. E. Lamers, R. Van Kruchten, T. Mastenbroek, C. Baaten, S. Coort, N. Pugh, A. Schulz, *et al.*, *Nat. Commun.*, 2014, **5**, 1.
38 W. Wu, D. Pott, B. Mazza, T. Sironi, E. Dordoni, C. Chiastra, L. Petrini, G. Pennati, G. Dubini, U. Steinseifer, *et al.*, *Ann. Biomed. Eng.*, 2016, **44**, 590.
39 Y. Chen and H. Luo, *J. Fluids Struct.*, 2018, **80**, 332.
40 D. Hernandez-Vaquero, C. Vigil-Escalera, Y. Persia, C. Morales, I. Pascual, A. Domínguez-Rodríguez, E. Rodríguez-Caulo, M. Carnero, R. Díaz, P. Avanzas, *et al.*, *J. Clin. Med.*, 2020, **9**, 1.

41 N. Kiesendahl, C. Schmitz, A. Von Berg, M. Menne, T. Schmitz-Rode, J. Arens and U. Steinseifer, *Ann. Biomed. Eng.*, 2020, **48**, 282.
42 N. Kiesendahl, C. Schmitz, M. Menne, T. Schmitz-Rode and U. Steinseifer, *Ann. Biomed. Eng.*, 2021, **49**, 885.
43 L. Chen, C. Yan and Z. Zheng, *Mater. Today*, 2018, **21**, 38.
44 F. Monie, B. Grignard and C. Detrembleur, *ACS Macro Lett.*, 2022, **11**, 236.
45 C. Pronoitis, M. Hakkarainen and K. Odelius, *ACS Sustainable Chem. Eng.*, 2022, **10**, 2522.
46 K. N. Raftopoulos, I. Łukaszewska, C. Bujalance Calduch, P. Stachak, S. Lalik, E. Hebda, M. Marzec and K. Pielichowski, *Polymer*, 2022, **253**, 125010.
47 B. V. K. J. Schmidt, *Polymers*, 2019, **11**, 693.
48 B. Niemczyk-Soczynska, A. Gradys and P. Sajkiewicz, *Polymers*, 2020, **12**(11), 2636.
49 D. C. Aduba, K. Zhang, A. Kanitkar, J. M. Sirrine, S. S. Verbridge and T. E. Long, *J. Appl. Polym. Sci.*, 2018, **135**, 46464.
50 D. Visser, H. Bakhshi, K. Rogg, E. Fuhrmann, F. Wieland, K. Schenke-Layland, W. Meyer and H. Hartmann, *ACS Omega*, 2022, **7**(44), 39772–39781.
51 J. J. Warner, P. Wang, W. M. Mellor, H. H. Hwang, J. H. Park, S.-H. Pyo and S. Chen, *Polym. Chem.*, 2019, **10**, 4665.
52 N. Fanjul-Mosteirín, R. Aguirresarobe, N. Sadaba, A. Larrañaga, E. Marin, J. Martin, N. Ramos-Gomez, M. C. Arno, H. Sardon, A. P. Dove, *et al.*, *Chem. Mater.*, 2021, **33**, 7194.
53 S. K. Pramanik, S. Sreedharan, H. Singh, M. Khan, K. Tiwari, A. Shiras, C. Smythe, J. A. Thomas and A. Das, *Bioconjugate Chem.*, 2018, **29**, 3532.
54 N. Esmaeili, M. J. Zohuriaan-Mehr, A. Salimi, M. Vafayan and W. Meyer, *Thermochim. Acta*, 2018, **664**, 64.
55 Y. Zhao, X. Xia, J. Zhou, Z. Huang, F. Lei, X. Tan, D. Yu, Y. Zhu and H. Xu, *Adv. Compos. Hybrid Mater.*, 2022, **1**, 3.
56 W. Xu, B. Liu, X. Cai, M. Zhang, X.-H. Zhang, P. Yu and X. H. Zhang, *J. Appl. Polym. Sci.*, 2018, **135**, 40.
57 R. Gharibi, M. B. Teimouri and S. Safavian, *Surf. Coat. Technol.*, 2022, **429**, 127925.
58 Y. Wu, *Thromb. J.*, 2015, **13**, 1.
59 S. K. Jaganathan and M. Mohan Prasath, *Biomed. Res.*, 2017, **28**, 5107.
60 W. Geerts, *Hematology*, 2014, **2014**, 306.
61 J. H. Spühler, J. Jansson, N. Jansson and J. Hoffman, *Front. Physiol.*, 2018, **9**, 340464.
62 M. Nowak, E. Divo and W. P. Adamczyk, *Int. J. Mech. Sci.*, 2022, **227**, 107410.
63 G. Luraghi, F. Migliavacca and J. F. Rodriguez Matas, *Cardiovasc. Eng. Technol.*, 2018, **9**, 723.
64 G. Luraghi, W. Wu, F. De Gaetano, J. F. Rodriguez Matas, G. D. Moggridge, M. Serrani, J. Stasiak, M. L. Costantino and F. Migliavacca, *J. Biomech.*, 2017, **58**, 45.
65 R. Zakerzadeh, M. C. Hsu and M. S. Sacks, *Expert Rev. Med. Devices*, 2017, **14**, 849.
66 H. T. Bui, A. Ishrat, S. P. James and L. P. Dasi, *J. Mech. Behav. Biomed. Mater.*, 2022, **135**, 105434.
67 J. H. Lee, A. D. Rygg, E. M. Kolahdouz, S. Rossi, S. M. Retta, N. Duraiswamy, L. N. Scotten, B. A. Craven and B. E. Griffith, *Ann. Biomed. Eng.*, 2020, **48**, 1475.
68 T. B. Le, M. Usta, C. Aidun, A. Yoganathan and F. Sotiropoulos, *Fluids*, 2022, **7**(3), 94.
69 O. M. Rotman, B. Kovarovic, W. C. Chiu, M. Bianchi, G. Marom, M. J. Slepian and D. Bluestein, *Ann. Biomed. Eng.*, 2019, **47**, 113.
70 S. Kaule, S. Pfensig, S. Siewert, K. P. Schmitz, M. Stiehm, S. Kohse, N. Grabow and A. Öner, *Curr. Dir. Biomed. Eng.*, 2019, **5**, 473.
71 G. Rokicki, P. G. Parzuchowski and M. Mazurek, *Polym. Adv. Technol.*, 2015, **26**, 707.
72 N. L. Tai, M. Ghasemlou, R. Adhikari and B. Adhikari, *Carbohydr. Polym.*, 2021, **265**, 118029.
73 S. Benyahya, M. Desroches, R. Auvergne, S. Carlotti, S. Caillol and B. Boutevin, *Polym. Chem.*, 2011, **2**, 2661.
74 V. Besse, R. Auvergne, S. Carlotti, G. Boutevin, B. Otazaghine, S. Caillol, J. P. Pascault and B. Boutevin, *React. Funct. Polym.*, 2013, **73**, 588.
75 J. L. J. van Velthoven, L. Gootjes, D. S. van Es, B. A. J. Noordover and J. Meuldijk, *Eur. Polym. J.*, 2015, **70**, 125–135.
76 H. T. Bui, N. Khair, B. Yeats, S. Gooden, S. P. James and L. P. Dasi, *Adv. Healthcare Mater.*, 2021, **10**, 1.
77 M. Heitkemper, H. Hatoum and L. P. Dasi, *J. Mech. Behav. Biomed. Mater.*, 2019, **98**, 163.
78 M. Bähr and R. Mülhaupt, *Green Chem.*, 2012, **14**, 483.
79 A. Pierrard, A. Aqil, C. Detrembleur and C. Jérôme, *Biomacromolecules*, 2023, **24**, 10.
80 J. W. M. Heemskerk, J. P. van Geffen, S. L. N. Brouns, J. Batista, H. McKinney, C. Kempster, M. Nagy, S. Sivapalaratnam, C. C. F. M. J. Baaten, K. Downes, *et al.*, *Haematologica*, 2019, **104**(6), 1256–1267.
81 A. Quarteroni, M. Tuveri and A. Veneziani, *Comput. Vis. Sci.*, 2000, **2**, 163.
82 E. S. Di Martino, G. Guadagni, A. Fumero, G. Ballerini, R. Spirito, P. Biglioli and A. Redaelli, *Med. Eng. Phys.*, 2001, **23**, 647.

